Supporting information

A 3D-printed hierarchical porous architecture of MOF@clay composite for rapid and highly efficient dye scavenging

*Hossein Shahriyari Far[1], Mina Najafi[1], Mahdi Hasanzadeh[*2], Rahmatollah Rahimi[*1]*

[1]Department of Chemistry, Iran University of Science and Technology, P.O. Box, Narmak 16846-13114, Tehran, Iran.

[2]Department of Textile Engineering, Yazd University, P.O. Box, 89195-741 Yazd, Iran.

Corresponding authors:

Mahdi Hasanzadeh, E-mail: m.hasanzadeh@yazd.ac.ir; Tel: +98-353-1232569; Fax: +98-353-8209817;

Rahmatollah Rahimi, E-mail: Rahimi_Rah@iust.ac.ir;

Table of content:

Figure S1. The EDS spectra and the Cr elemental mapping image of the MOF@Clay composite.

Figure S2. The elemental mapping image of the 3D-MOF@Clay architecture.

Figure S3. TGA curve of the MOF@Clay composite.

Figure S4. Zeta-potential of 3D-MOF@Clay architecture.

Figure S5. The chemical structure and molecular size of MO and DR31 dyes.

Figure S6. Comparison of dye removal efficiency of 3D-CS and 3D-MOF@Clay architectures toward (a) MO and (b) DR31 dyes.

Figure S7. The plots of non-linear Langmuir, Freundlich, Temkin, and Dubbin-Radushkevich isotherm models for adsorption of (a) DR31 and (b) MO dyes on the 3D-MOF@Clay architecture (pH = 4, 3D-MOF@Clay = 2.4 g, contact time = 60 min).

Figure S8. The plots of (a,b) non-linear PFO and PSO models, and (c,d) intraparticle diffusion model for adsorption of (a,c) DR31 and (b,d) MO dyes on the 3D-MOF@Clay architecture (pH = 4, dye concentration= 60 ppm, 3D-MOF@Clay = 2.4 g).
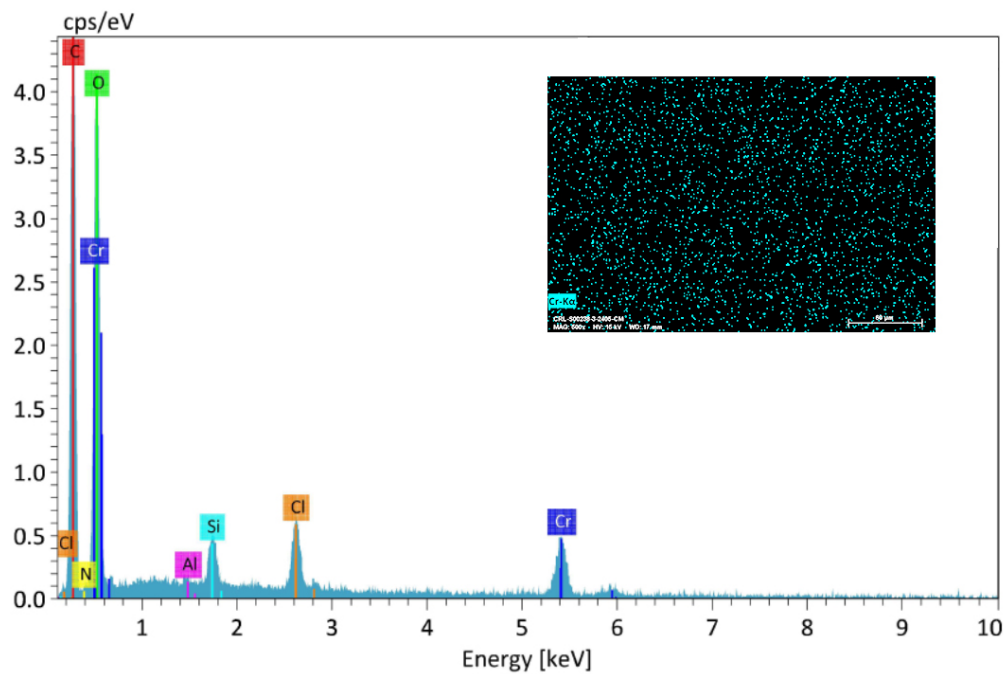
Figure S1. The EDS spectra and the Cr elemental mapping image of the MOF@Clay composite.
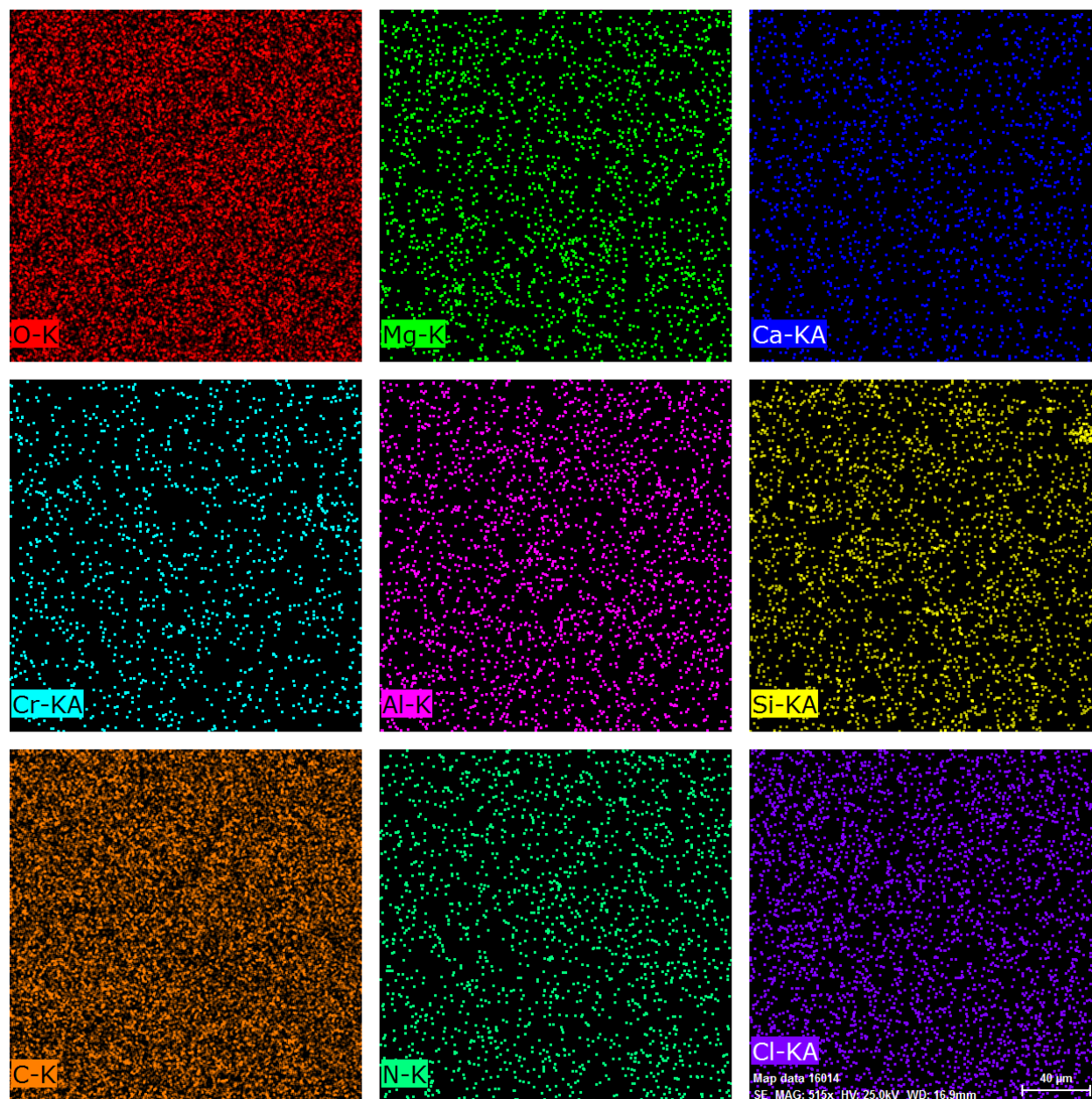
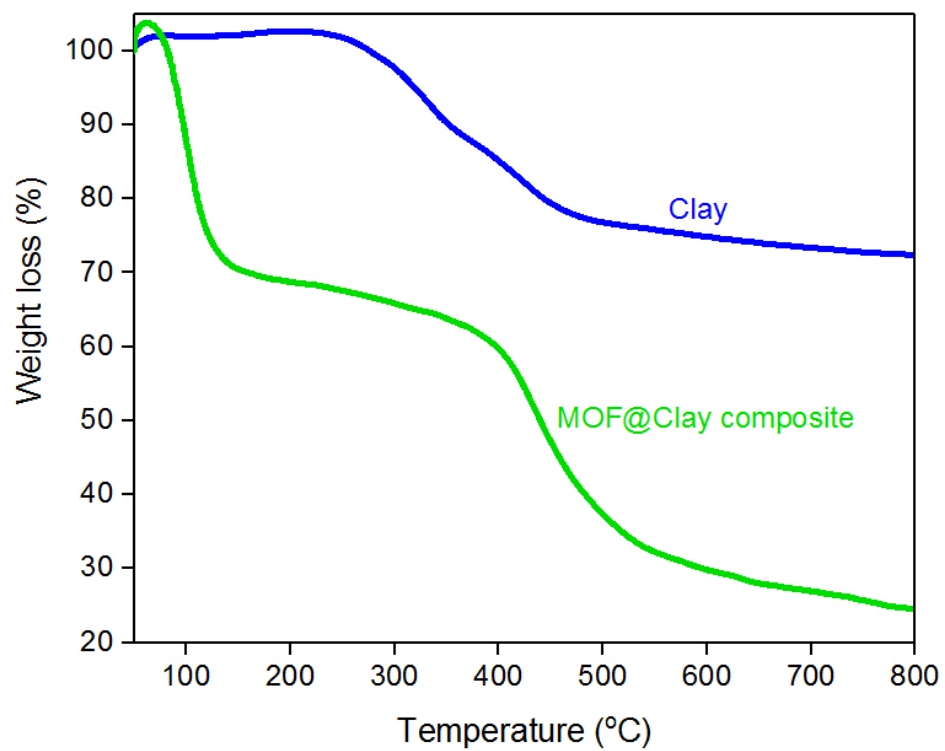**Figure S2.** The elemental mapping image of the 3D-MOF@Clay architecture.
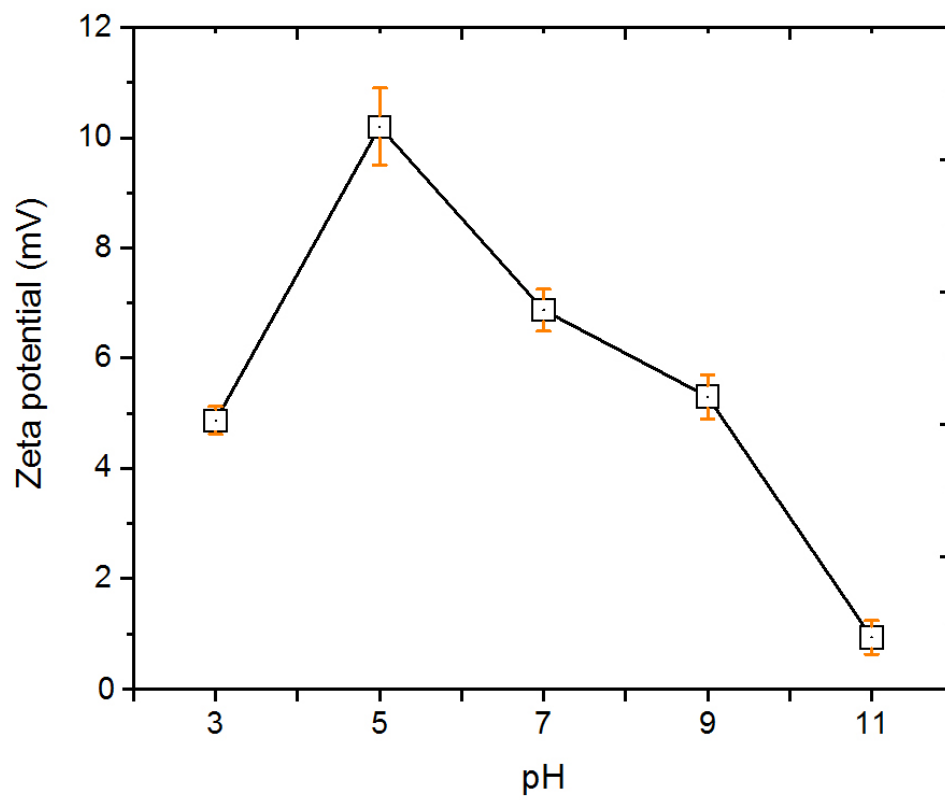
Figure S3. TGA curve of the MOF@Clay composite.

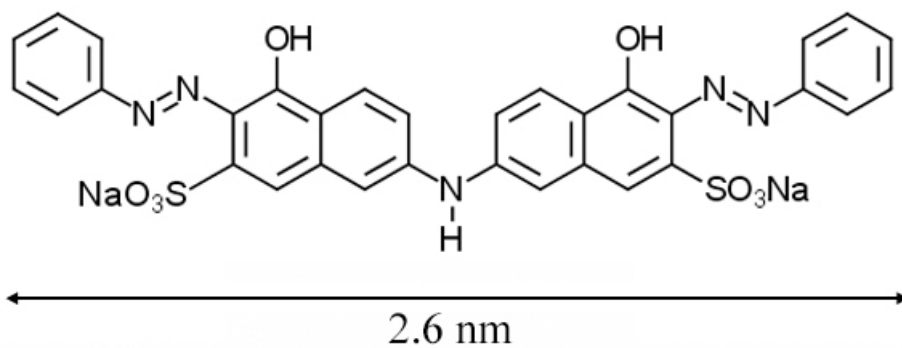**Figure S4.** Zeta-potential of 3D-MOF@Clay architecture.

Direct Red 31 (DR31)
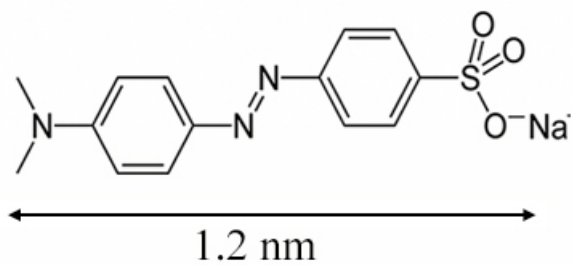

2.6 nm

Methyl Orange (MO)

1.2 nm

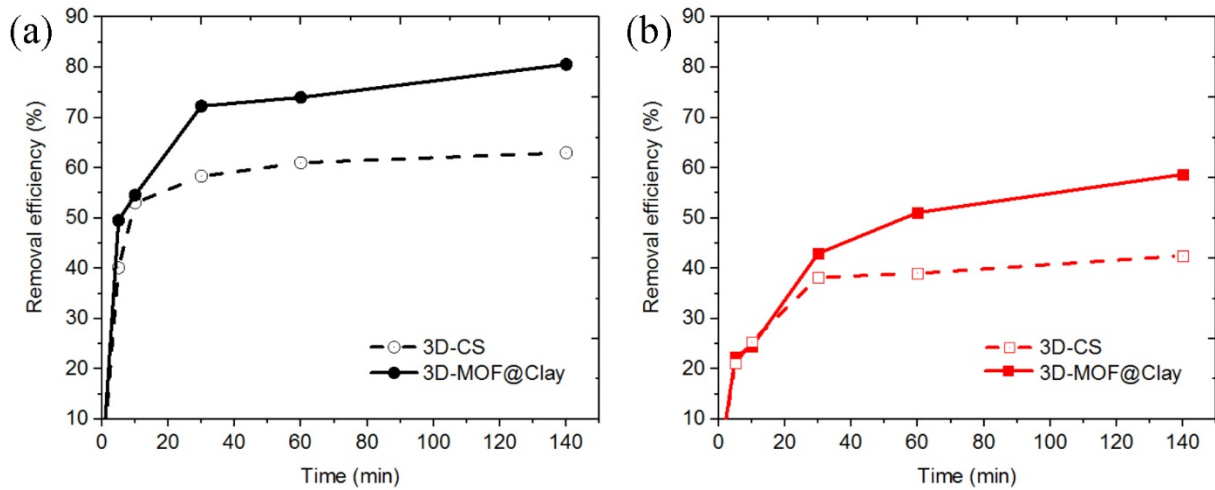**Figure S5.** The chemical structure and molecular size of MO and DR31 dyes.

Figure S6. Comparison of dye removal efficiency of 3D-CS and 3D-MOF@Clay architectures toward (a) MO and (b) DR31 dyes.

ES1: Adsorption isotherm

Adsorption isotherms were obtained through the fitting of experimental data with Langmuir, Freundlich, Temkin, and Dubinin-Radushkevich (DRK) isotherm models. The non-linear form of isotherm models are expressed by the following equations [1, 2]:

$$q_e = \frac{q_{max} K_L C_e}{1 + K_L C_e} \tag{5}$$

$$q_e = k_F C_e^{\frac{1}{n}} \tag{6}$$

$$q_e = B \ln(K_T C_e) \tag{7}$$

$$q_e = (q_{max}) \exp(-\beta \varepsilon^2) \tag{8}$$

where C_e (mg/L) is the dye concentration at equilibrium. K_L (L/mg) and K_F ((mg/g)(L/mg)$^{1/nF}$) are the Langmuir and Freundlich constants, respectively. $1/n$ is related to the adsorption intensity [3, 4]. B (J/mol) and K_T (L/mg) are the Temkin constants. β (mol^2/kJ^2) and ε (kJ/mol) are also the adsorption energy and adsorption potential constants, respectively [5]
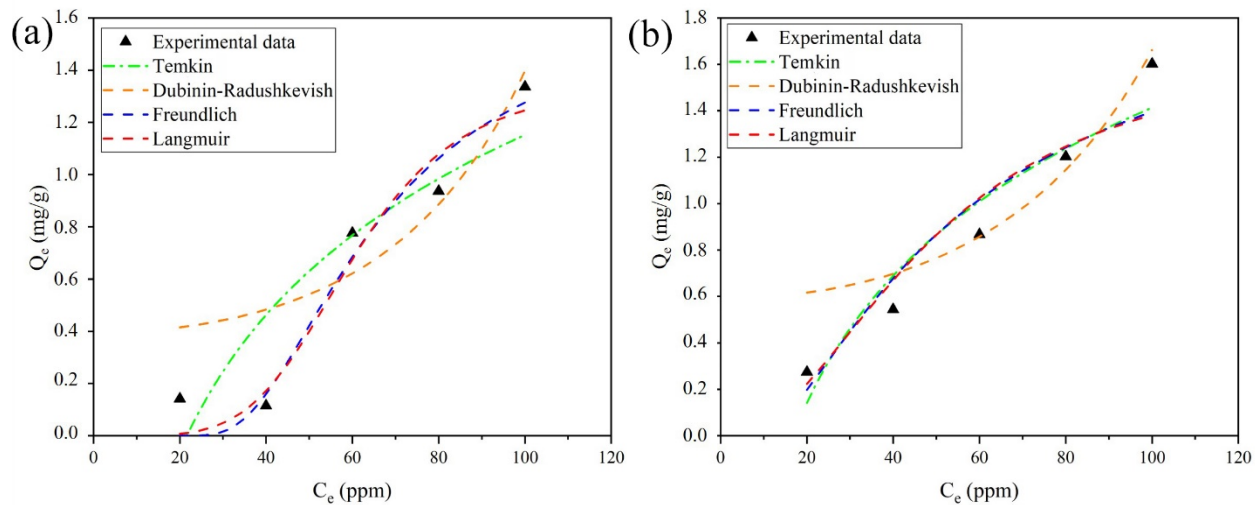
Figure S7. The plots of non-linear Langmuir, Freundlich, Temkin, and Dubbin-Radushkevich

isotherm models for adsorption of (a) DR31 and (b) MO dyes on the 3D-MOF@Clay

architecture (pH = 4, 3D-MOF@Clay = 2.4 g, contact time = 60 min).

ES2: Adsorption kinetics

The kinetics of dye adsorption on 3D-MOF@Clay architecture were evaluated by non-linear pseudo-first-order, non-linear pseudo-second-order, and intraparticle diffusion models based on the following equations [6, 7]:

$$q_t = q_e(1 - e^{-k_1 t})$$
(2)

$$q_t = \frac{k_2 q_e^2 t}{1 + k_2 q_e t}$$
(3)

$$q_t = K_P t^{0.5} + I$$
(4)

where q_t and q_e are adsorption capacity at the time t and equilibrium, respectively. k_1 (1/min), and k_2 (g/mg.min) are also the rate constant of pseudo-first-order and pseudo-second-order models, respectively. K_P (mg/g.min$^{0.5}$) and I are the rate constant of the IPD model and the thickness of the boundary layer, respectively.
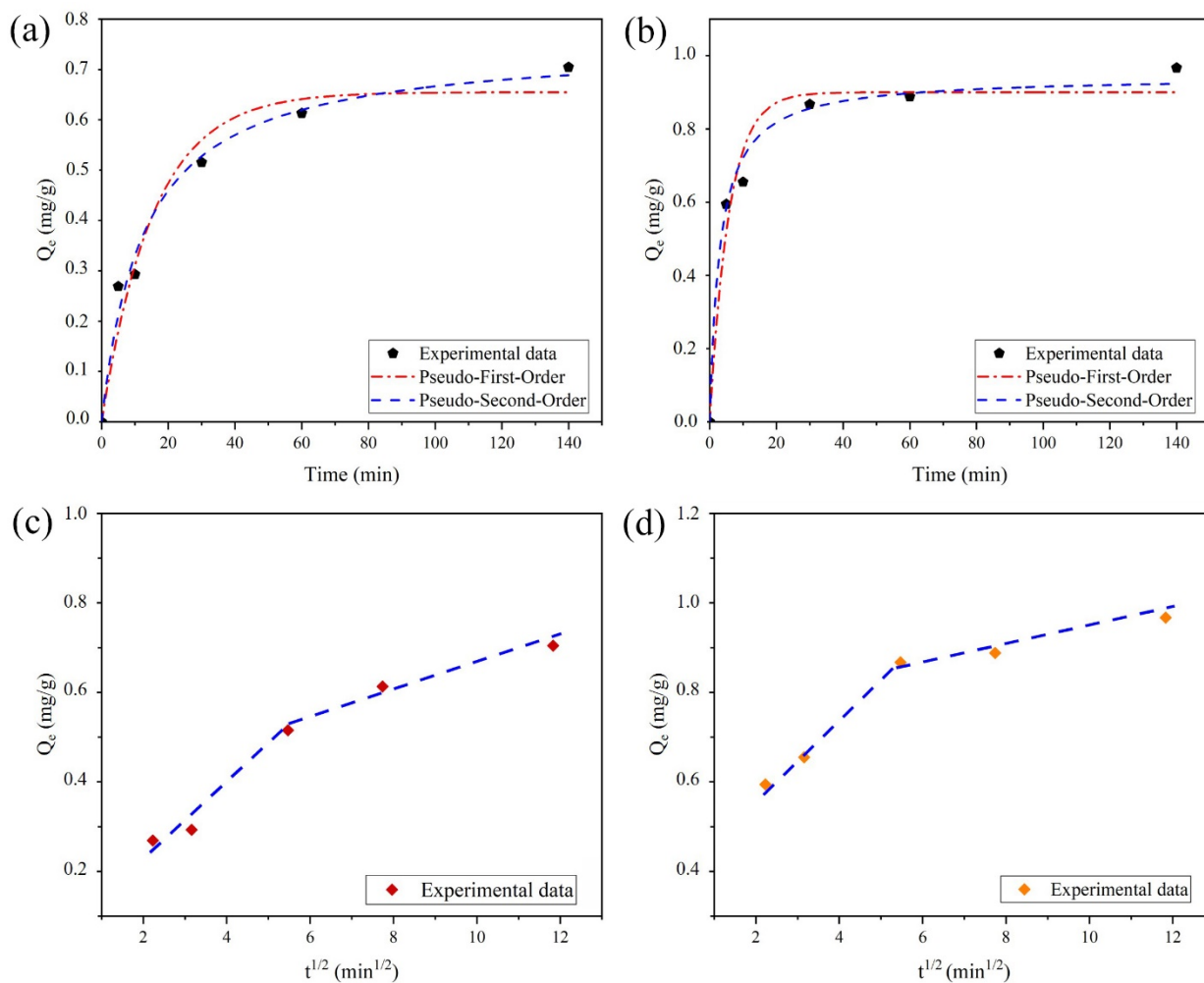
Figure S8. The plots of (a,b) non-linear PFO and PSO models, and (c,d) intraparticle diffusion model for adsorption of (a,c) DR31 and (b,d) MO dyes on the 3D-MOF@Clay architecture (pH = 4, dye concentration= 60 ppm, 3D-MOF@Clay = 2.4 g).

References:

1. Raeiszadeh M, Hakimian A, Shojaei A, Molavi H (2018) Nanodiamond-filled chitosan as an efficient adsorbent for anionic dye removal from aqueous solutions. J Environ Chem Eng 6:3283–3294

2. Bayazit ŞS, Yildiz M, Aşçi YS, Şahin M, Bener M, Eğlence S, Abdel Salam M (2017) Rapid adsorptive removal of naphthalene from water using graphene nanoplatelet/MIL-101 (Cr) nanocomposite. J Alloys Compd. https://doi.org/10.1016/j.jallcom.2017.01.111

3. Heydari Moghaddam M, Nabizadeh R, Dehghani MH, Akbarpour B, Azari A, Yousefi M (2019) Performance investigation of Zeolitic Imidazolate Framework – 8 (ZIF-8) in the removal of trichloroethylene from aqueous solutions. Microchem J 150:104185

4. Baziar M, Zakeri HR, Ghalehaskar S, Nejad ZD, Shams M, Anastopoulos I, Giannakoudakis DA, Lima EC (2021) Metal-organic and Zeolitic imidazole frameworks as cationic dye adsorbents: physicochemical optimizations by parametric modeling and kinetic studies. J Mol Liq 332:115832

5. Hu Q, Zhang Z (2019) Application of Dubinin–Radushkevich isotherm model at the solid/solution interface: A theoretical analysis. J Mol Liq 277:646–648

6. Saucier C, Karthickeyan P, Ranjithkumar V, Lima EC, dos Reis GS, de Brum IAS (2017) Efficient removal of amoxicillin and paracetamol from aqueous solutions using magnetic activated carbon. Environ Sci Pollut Res 24:5918–5932

7. Lin J, Wang L (2009) Comparison between linear and non-linear forms of pseudo-first-order and pseudo-second-order adsorption kinetic models for the removal of methylene blue by

activated carbon. Front Environ Sci Eng China 3:320–324